Investigation of ion cyclotron range of frequencies mode conversion at the ion–ion hybrid layer in Alcator C-Mod[a)]

Y. Lin,[b)] S. Wukitch, P. Bonoli, E. Nelson-Melby,[c)] M. Porkolab, J. C. Wright, N. Basse, A. E. Hubbard, J. Irby, L. Lin, E. S. Marmar, A. Mazurenko,[d)] D. Mossessian, A. Parisot, J. Rice, and S. Wolfe
MIT, Plasma Science and Fusion Center, Cambridge, Massachusetts 02139

C. K. Phillips, G. Schilling, and J. R. Wilson
Plasma Physics Laboratory, Princeton, New Jersey 08540

P. Phillips and A. Lynn
Fusion Research Center, University of Texas, Austin, Texas 78712

(Received 22 October 2003; accepted 16 December 2003; published online 23 April 2004)

Mode conversion (MC) of long wavelength fast electromagnetic magnetosonic waves (fast wave, or FW) into shorter wavelength electrostatic (ion-Bernstein, or IBW) or slow electromagnetic (ion cyclotron, or ICW) waves is of great interest in laboratory, magnetic fusion and space physics experiments. Such processes are particularly important in multi-ion species plasmas. In this paper we report recent results from high power ion cyclotron range of frequencies (ICRF) heating experiments in the Alcator C-Mod tokamak. Mode converted waves near the ^{3}He–H hybrid layer have been detected by means of phase contrast imaging in H(^{3}He,D) plasmas [E. Nelson-Melby *et al.*, Phys. Rev. Lett. **90**, 155004 (2003)]. The measured wave k spectrum and spatial location are in agreement with theoretical predictions [F. W. Perkins, Nucl. Fusion **17**, 1197 (1977)], which showed that in a sheared magnetic field, mode-conversion of FW into ICW may dominate over IBW for appropriate ion species (i.e., D–T, or equivalently, H–^{3}He). Recent modeling with full wave codes, as well as solving the hot plasma dispersion equation in the presence of sheared magnetic fields, verifies the interpretation of such a mode conversion process. Thus, the geometry of the magnetic field, as well as the particular ion species mix, influences the physics of ICRF mode conversion. In this paper, we also report recent results on the study of mode conversion electron heating (MCEH) in D(H) plasmas [Y. Lin *et al.*, Plasmas Phys. Controlled Fusion **45**, 1013 (2003)]. By comparing the experimentally measured MCEH profile with modeling, the study shows that the MC ICW may make a significant contribution to the direct electron heating when the D–H hybrid layer is off axis on the high field side. Preliminary results of mode conversion poloidal plasma flow drive experiments in D(^{3}He) are also reported. © *2004 American Institute of Physics.*
[DOI: 10.1063/1.1651489]

I. INTRODUCTION

Mode conversion (MC) of long wavelength fast electromagnetic magnetosonic waves (fast wave, or FW) into shorter wavelength electrostatic (ion-Bernstein, or IBW) or slow electromagnetic (ion cyclotron, or ICW) waves is of great interest in laboratory, magnetic fusion and space physics experiments. Such processes are particularly important in multi-ion species plasmas. In tokamak experiments with ion cyclotron range of frequencies (ICRF) heating, the mode conversion process has been extensively studied as a tool for direct electron heating and current drive.[1–8] It has also been shown possibly to drive poloidal plasma flow,[9] and potentially suppress turbulence. Therefore, understanding the ICRF MC physics is important to the study of the advanced tokamak operation scenario.

In a multi-species plasma, the dispersion equation of the fast wave in the cold plasma limit can be written as

$$n_\perp^2 = \frac{(R-n_\parallel^2)(L-n_\parallel^2)}{S-n_\parallel^2}, \tag{1}$$

where R, L and S are the usual Stix parameters,[10] $n_\parallel = ck_\parallel/\omega$ and $n_\perp = ck_\perp/\omega$ are the parallel and perpendicular index of refraction, respectively. Two cutoff layers, $n_\parallel^2 = R$ and $n_\parallel^2 = L$, and a resonance layer, $n_\parallel^2 = S$ (ion–ion hybrid layer) are present in Eq. (1). The ion–ion hybrid layer is located between the two ion cyclotron (IC) layers. The distances to the IC layers are determined by the species mix. For example, in a D(H) plasma with H as the minority species, the D–H hybrid layer is closer to the H IC layer than the D IC layer. In contrast to the pure right hand polarization in single species plasmas, the polarization of the fast wave is partially left hand near the hybrid layer. This modification of

[a)]Paper GI2 5, Bull. Am. Phys. Soc. **48**, 127 (2003).
[b)]Invited speaker. Electronic mail: ylin@psfc.mit.edu
[c)]Present address: 1110 E. Drachman St., Tucson, AZ 85719.
[d)]Present address: Phillips Advanced Metrology Systems, Inc., Natick, MA 01760.

polarization is the essence of the ICRF minority heating scheme. In a D(H) plasma with only a few percent of H, the fast wave will be mostly absorbed at the H IC layer, which is Doppler broadened to overlap the D–H hybrid layer with the help of the energetic H particles generated by the rf power. With a moderate H concentration, the D–H hybrid layer may be out of the IC broadening. As a result, the single-pass absorption of the fast wave becomes weak, and the fast wave may be converted to shorter wavelength waves in the vicinity of the hybrid layer. There are generally two types of MC waves in this region. One is the electrostatic ion-Bernstein wave (IBW) on the high field side (HFS) of the ion–ion hybrid layer. On the low field side (LFS) of the layer, the slow electromagnetic ion cyclotron wave (ICW) of the species with higher charge/mass ratio may appear because of the upshift of the $k_{\|}$ of the fast wave induced by the magnetic shear, like that created by the poloidal field (B_{pol}) in tokamaks.[11] Without B_{pol}, the ICW can exist only in a small region near the edge of a multi-species tokamak plasma. The upshift of $k_{\|}$ provides a mechanism for the expansion of this edge region further into the plasma. After its existence in tokamak plasmas was shown in Ref. 11, the MC ICW was only considered in the scenario that the fast wave is launched from the HFS of the ion–ion hybrid layer. For the usual LFS launch fast wave, the MC IBW was thought of as the only possible MC wave. In reality, the presence of the $n_{\|}^2 = R$ cutoff layer in the HFS edge plasma suggests that the MC ICW should also exist for the LFS launch fast wave. The MC ICW in tokamak plasmas has recently been observed experimentally for the first time by means of a phase contrast imaging (PCI) system in H(^{3}He,D) plasmas in Alcator C-Mod.[12] The experimental observation was compared with numerical studies, which helped identify the observed wave. The MC ICW usually has a longer wavelength than the MC IBW, but shorter wavelength than the fast wave. In contrast to the MC IBW, which is a warm plasma wave, the MC ICW is the competition result of B_{pol} and temperature.[13] This experimental observation of the MC ICW, as well as a recent numerical study,[14] suggests that ICRF mode conversion in tokamak plasmas is more complicated than previously thought.

A further study of the MC process in Alcator C-Mod has been performed on the direct electron heating (MCEH) of the MC waves in D(H) plasmas.[15] The MCEH profile and efficiency as calculated from experimental data agree with those from numerical simulations. The contributions from the MC ICW and MC IBW are examined. The result suggests that the contribution from the MC ICW can be significant when the ion–ion hybrid layer is off axis on the HFS of the magnetic axis, where B_{pol} is non-negligible.

Plasma flow drive using ICRF waves has been studied theoretically[14,16–20] and experimentally[9,21–23] in different tokamaks and utilizing either direct launch IBW or MC waves. Flow drive through externally applied rf waves is thought as a potential ''knob'' to enhance plasma confinement.[24] Direct-launch IBW has been shown to drive plasma flow[21] and enhance plasma confinement.[22–25] Poloidal flow drive based on mode conversion has been studied in D(^{4}He, ^{3}He) plasmas in the Tokamak Fusion Test Reactor (TFTR),[9] in which an rf power correlated poloidal flow was observed on the LFS of the D–^{3}He hybrid layer. Some experiments have also been performed in Alcator C-Mod to investigate the MC flow drive. Preliminary results are reported in this paper.

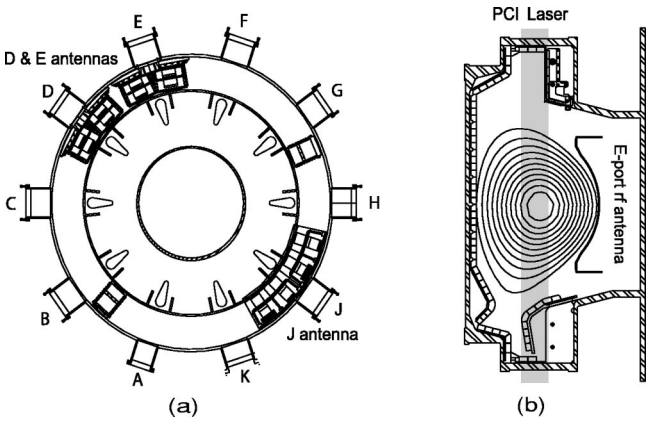

FIG. 1. (a) Fast wave antennas shown in the top view of Alcator C-Mod. (b) The PCI system shown in a cross section of Alcator C-Mod.

This paper is organized as follows: Sec. II summarizes the experimental observation of the MC ICW and the numerical studies to identify its origin; Sec. III presents the MCEH study in D(H) plasmas; and Sec. IV reports some preliminary results of MC flow drive experiments in Alcator C-Mod, followed by Summary.

II. OBSERVATION OF THE MODE CONVERTED ION CYCLOTRON WAVE

Alcator C-Mod ($R \simeq 0.67$ m, $a \simeq 0.22$ m, $B_t \leqslant 8.1$ T)[26] has three fast wave antennas [Fig. 1(a)]: two two-strap antennas at D port ($f = 80.5$ MHz) and E port ($f = 80$ MHZ),[27] and a four-strap antenna at J port.[28] The J antenna was operated at either 70 or 78 MHz in the experiments reported in this paper.

In Fig. 1(b), we also show the PCI system,[29] a laser based density fluctuations diagnostic in Alcator C-Mod. The CO_2 laser ($\lambda = 10.6$ nm) of PCI is vertically in front of the E antenna. The laser light is imaged onto a 12-element HgCdTe photoconductive linear array after passing through the plasma and reflected from a 90° phase plate. The PCI technique[30] relies on the interference of scattered and appropriately phase-shifted un-scattered radiation passing through the plasma. It is most sensitive to density perturbations whose surfaces of constant phase are aligned with the laser beam. In experiments with a special mix of D, ^{3}He and H, a wave with k_R in the range of $+4$ to $+10$ cm^{-1}, where R is the tokamak major radius, is observed by PCI. In Fig. 2, we plot the k-spectrum contour from the PCI signal of one of the plasma discharges in these experiments. A wave at $k_R \simeq +7$ cm^{-1} is clearly shown. The plasma parameters are: $B_\phi = 5.84$ T, $I_p = 800$ kA, $n_{\mathrm{H}}/n_e \simeq 0.59$, $n_{^3\mathrm{He}}/n_e \simeq 0.04$, $n_{\mathrm{D}}/n_e \simeq 0.33$, $n_{e0} \simeq 2 \times 10^{20}$ m^{-3}, and $T_{e0} \simeq 1.3$ keV. In these experiments, the PCI laser was expanded to a width of about 6 cm, and configured as a heterodyne system: the laser intensity was modulated at a frequency offset from the rf frequency so that the rf signals (e.g., 80.5 MHz from the D

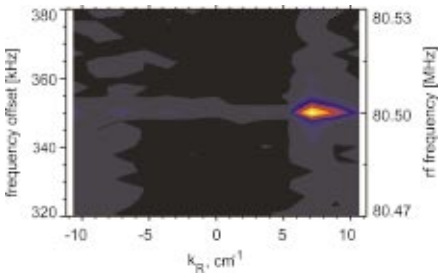

FIG. 2. (Color) Contour plot of PCI signals in frequency and k_R space.

antenna) could be measured at the beat oscillation frequency (350.9 kHz) (Fig. 2). The wave is located in the vicinity but on the LFS of the ^{3}He–H hybrid layer (Fig. 3). The positive k_R shown in Fig. 2 indicates that the phase velocity of the wave is toward the antenna. The wave also has a longer wavelength than that of the MC IBW (wavelength of a few mm) expected on the HFS of the ^{3}He–H hybrid layer.

In Fig. 4, the dispersion curves of the fast wave, ICW and IBW near the ^{3}He–H hybrid layer for the plasma of Fig. 2 are plotted. The dispersion curves are numerically obtained by solving the full electromagnetic dispersion equation assuming a Maxwellian plasma.[31] The FW and IBW curves are obtained on the midplane without including the poloidal field. The ICW is obtained along the magnetic surface tangential to the ^{3}He–H hybrid layer on the midplane. The poloidal field provides the mechanism for the upshift of $k_\parallel$.[32] Assuming $k_r \ll k_{\rm pol}$ and $k_\perp \simeq k_{\rm pol}$, we have

$$k_\parallel \simeq \frac{n_\phi}{R}\frac{B_\phi}{B_{\rm total}} + k_\perp \frac{B_{\rm pol}}{B_{\rm total}}, \tag{2}$$

where toroidal mode number $n_\phi = 10$ is conserved due to the toroidal symmetry. In Fig. 5(a), we plot both the real, Re($k_\perp$), and imaginary, Im($k_\perp$), parts of the wave number of the ICW branch of Fig. 4. We also plot the resulted $k_\perp$ from solving Eq. (2) in conjunction with an approximate slow wave root[33]

$$n_\perp^2 \simeq (S - n_\parallel^2)/\sigma, \tag{3}$$

where $\sigma \simeq -(\epsilon_{xx} - S)/n_\perp^2$ is the hot plasma correction of the Stix parameter S, and ϵ_{xx} is the xx component of the hot plasma dielectric tensor. Equation (3) is also an approximate expression of the MC IBW on the HFS of the hybrid layer.[4] The two sets of curves shown in Fig. 5(a) are very close and

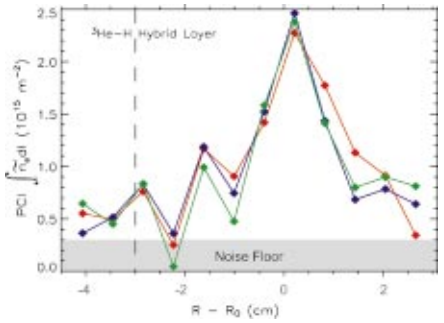

FIG. 3. (Color) PCI raw signal levels at the rf beat frequency vs $R - R_0$, where R_0 is the major radius of the magnetic axis. Three curves are signals at three different time points.

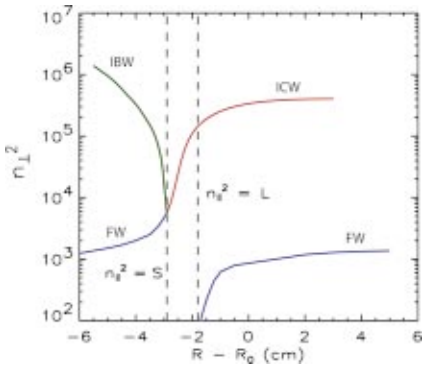

FIG. 4. (Color) Dispersion curves of the FW, ICW, and IBW for the plasma of Fig. 2.

both show a damped wave with Re($k_\perp$) in the same range as measured by PCI (cf. Fig. 2). A contour plot of the E_z component from a TORIC[34,35] simulation ($n_\phi = 10$) for this plasma is shown in Fig. 5(b). A short wavelength wave structure appears on the LFS of the ^{3}He–H hybrid layer. Its wavelength is in agreement with that shown in Fig. 5(a) and measured by PCI. A similar result has also been obtained by simulations using AORSA.[14] The up–down asymmetry of the wave front of the MC ICW [Fig. 5(b)] is a consequence of the fact that the wave propagates to the LFS of the mode conversion layer, which corresponds to positive m numbers ($k_{\rm pol} r$) below the midplane and negative m numbers above. For a positive $B_{\rm pol}$ and n_ϕ, the positive m numbers below the midplane result in larger values of $k_\parallel$ that the local dispersion relation admits as a propagating ICW [cf. Eq. (2)]. In contrast, the negative m numbers above the midplane yield reduced values of $k_\parallel$ that are evanescent modes of the local dispersion relation. Because $|E_z|/|E_y| \simeq k_\perp k_\parallel v_{\rm te}^2/2\omega\omega_{\rm ce}$,[36] the E_z field in the MC ICW is much stronger than that of FW or the MC IBW due to its large $k_\perp$ and $k_\parallel$ (Fig. 6). Because $\zeta = \omega/k_\parallel v_{\rm te} \leqslant 1$ (also shown in Fig. 6), the MC ICW is damped through electron Landau damping (ELD). Being left-hand

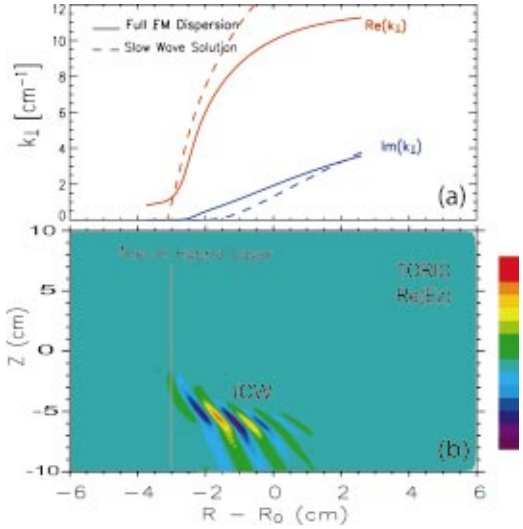

FIG. 5. (Color) Numerical studies of the MC ICW. (a) $k_\perp$ from full EM dispersion and from an approximate slow wave solution [Eq. (3)]. (b) Re(E_z) from TORIC simulation ($n_\phi = +10$).

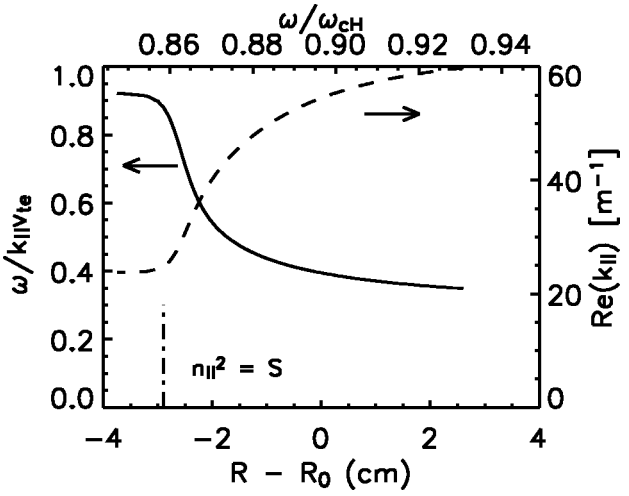

FIG. 6. $\omega/k_{\parallel}v_{te}$ (left) and $k_{\parallel}$ (right) of the MC ICW vs $R-R_0$ (bottom) and also $\omega/\omega_{\mathrm{cH}}$ (top).

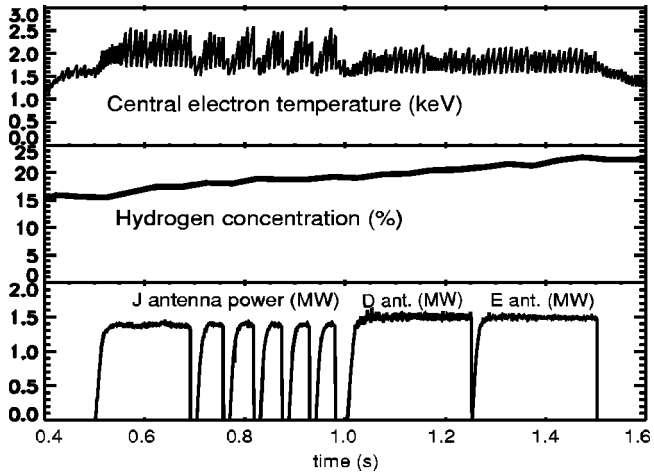

FIG. 7. Plasma parameter traces. $B_0 \simeq 5.4$ T, $I_p \simeq 1$ MA, $n_{e0} \simeq 1.8 \times 10^{20}$ m^{-3}. Antenna frequencies are 80.5, 80, and 70 MHz for D, E and J antennas, respectively.

polarized, the MC ICW will be completely absorbed through IC resonance if it ever reaches the H IC layer. In typical MC plasmas in Alcator C-Mod, the MC ICW can propagate in the order of several centimeters through ELD as shown by TORIC simulation, in agreement with the simple estimate in Ref. 11. The TORIC simulation and solutions from the dispersion equation both agree with the PCI observation with respect to the wave location and wavelength. In conclusion, the observed wave is identified as the MC ICW of the hydrogen species, the same slow wave branch as studied in a D–T mixture in Ref. 11 considering the poloidal field. It is the first experimental observation of the MC ICW in tokamak plasmas.[12]

III. MODE CONVERSION ELECTRON HEATING IN D(H) PLASMAS

Mode conversion electron heating, MCEH, has been studied in many tokamaks. In previous experiments in Alcator C-Mod, MCEH has been studied in detail in D(^{3}He) and H(^{3}He) plasmas,[3–5,37,38] and preliminarily in D(H) plasmas.[39] MCEH has also been studied in other tokamaks, e.g., D(^{3}He, ^{4}He)[2] and D(T) plasmas[1] in TFTR, ^{3}He(H) in ASDEX Upgrade[6] and Tore Supra,[7,40] and ^{4}He(^{3}He) in JET.[8] MCEH may be significant in D(H) plasmas with moderate hydrogen concentration in Alcator C-Mod as predicted in Ref. 41. Recently, a more detailed study of mode conversion in D(H) plasma has been performed.[15] In this experiment, we infer the H/D ratio from a spectroscopic diagnostic that measures hydrogen and deuterium Balmer α-line levels near the plasma edge.[42] A constant H/D ratio throughout the plasma is assumed. The MCEH profile is estimated from the following equation:

$$S(r) \simeq \frac{3}{2} n_e \Delta\left[\frac{\partial T_e(r)}{\partial t}\right], \tag{4}$$

where $\Delta[\partial T_e(r)/\partial t]$ is the difference of the slopes in the temperature signals before and after rf power transitions (break in slope).[43] The fraction of rf power to electron heating is simply $\eta_e \simeq \int S(r)dV/P_{\mathrm{total}}^{\mathrm{rf}}$ where the volume integration is performed based on the magnetic surfaces reconstructed by EFIT.[44] T_e is measured by a second harmonic heterodyne ECE system with high spatial resolution (<7 mm) and temporal response (5 μs).[45]

Figure 7 shows one of the typical plasma discharges in these experiments with a moderate H concentration. For this plasma, the rf power is applied consecutively by J (70 MHz), D (80.5 MHz) and E (80 MHz) antennas at a level about 1.5 MW. The D–H hybrid layer is nearly on axis when J port is on, while the layer is off axis on the high field side when D or E is on. The H concentration n_{H}/n_e is in the range of 0.15–0.25.

Figure 8 shows the experimentally obtained MCEH profile in comparison with the TORIC simulation result at $t = 0.8744$ s of the discharge in Fig. 7. The TORIC simulation is done with toroidal modes $n_\phi = \pm(9-17)$, and summed over all results by considering the antenna toroidal spectrum, which is peaked at $n_\phi = \pm 13$. A good agreement is shown between the experiments and simulation in the expected mode conversion region $0 < r/a < 0.25$. The MC fraction $\eta_e^{\mathrm{exp}} \simeq 0.16$ from the experimentally measured profile, and $\eta_e^{\mathrm{TORIC}} \simeq 0.14$ from the TORIC simulation. The minority heating profile from TORIC is also shown in this figure. The

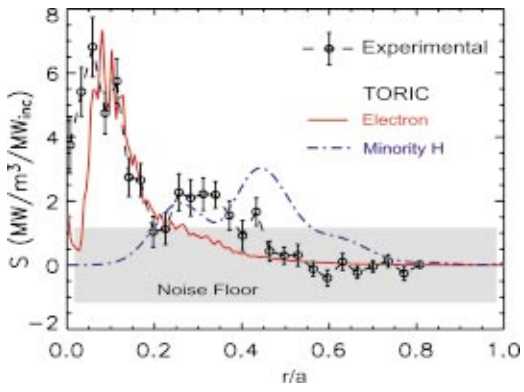

FIG. 8. (Color) MCEH profiles for the on-axis mode conversion ($t = 0.8744$ s, of the plasma in Fig. 7).

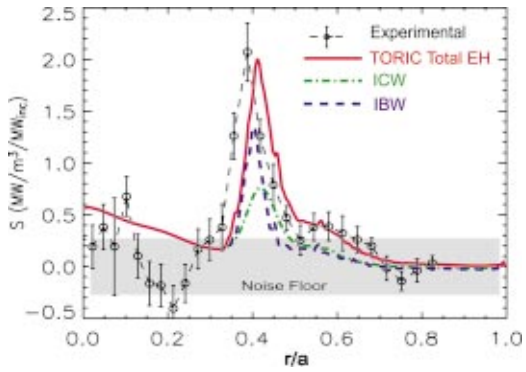

FIG. 9. (Color) MCEH profiles for the off-axis mode conversion ($t=1.5024$ s of the plasma in Fig. 7).

TORIC simulation shows that the direct electron heating power is primarily from the MC IBW. The result is consistent with the fact that B_{pol}, which is crucial for the excitation of the ICW, is small near the magnetic axis.

Figure 9 shows the MCEH profile obtained at $t=1.5024$ s in the same plasma discharge of Fig. 7. The E port antenna is on at 80 MHz with power level at about 1.5 MW. The D–H hybrid layer is off axis on the HFS at about $r/a=0.36$ for the dominant toroidal mode number $n_\phi=\pm 10$ of this antenna. The deposition profile from TORIC is also plotted. The TORIC simulation is done on $n_\phi=\pm(4-16)$. In the expected mode conversion region $0.35<r/a<0.7$, the volume integrated total MCEH power from the experiment is $\eta_e^{\mathrm{exp}}\simeq 0.20$, and $\eta_e^{\mathrm{TORIC}}\simeq 0.18$ from the TORIC simulation. The experimental result and TORIC result agree with each other in location, shape and level. We also show the power partition to MC ICW, MC IBW and FW electron heating from the TORIC simulation. The ICW and IBW peak at approximately the same r/a. The result suggests a comparable heating for the MC ICW $\eta_e^{\mathrm{ICW}}\simeq 0.087$ and MC IBW $\eta_e^{\mathrm{IBW}}\simeq 0.09$ while there is a small part of electron heating from the fast wave near the hydrogen cyclotron resonance on axis $\eta_e^{\mathrm{FW}}\simeq 0.03$.

In Fig. 10, the two-dimensional (2D) contour of power deposition S_{ELD} from the TORIC simulation ($n_\phi=10$) is plotted. The power deposition from the MC IBW and MC ICW is clearly shown, with the IBW on the HFS of the ion-ion hybrid layer and the ICW on the LFS. However, it is difficult to distinguish experimentally the MC ICW and IBW

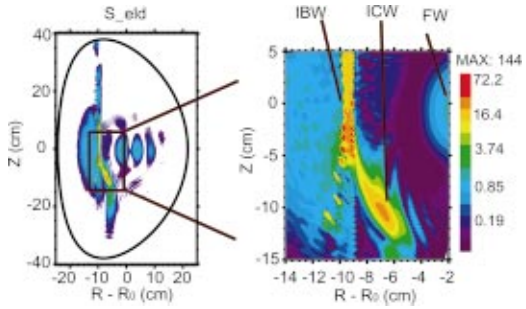

FIG. 10. (Color) Two-dimensional power deposition from TORIC for the off-axis MC ($n_\phi=10$). The unit of S_{ELD} is MW/m^3 per m^2 per MW antenna input power.

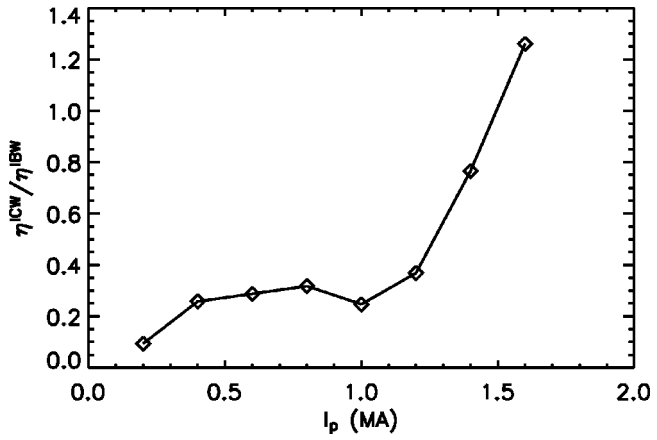

FIG. 11. Ratio of the MC ICW and MC IBW power from TORIC simulations ($n_\phi=10$) at different I_p. Other parameters are the same as those of Fig. 10.

contributions in direct electron heating because they generally peak at similar magnetic surfaces. The total MC efficiency and the power partition between the MC ICW and MC IBW are very complicated. They depend on a number of plasma parameters, such as plasma current, species mixture, density, and temperature. A high B_{pol} is favored by the MC ICW (Fig. 11).

IV. PRELIMINARY RESULTS OF MC FLOW DRIVE IN D(^{3}HE,H) PLASMAS

Experiments to study the mode conversion poloidal plasma flow drive have been performed on a limited number of D(^{3}He,H) plasmas in Alcator C-Mod. In Fig. 12, the rf power and poloidal velocity (v_{pol}) in one of the discharges (shot 10 307 160 20) are compared. The J port antenna was at 78 MHz and phasing predominantly at the countercurrent drive direction (waves travel in the co-current direction). In Fig. 12(a), the time traces of v_{pol} and the rf power from J-port antenna are plotted. A possible linear relation between these two parameters is shown in Fig. 12(b), which gives $v_{\mathrm{pol}}\simeq -18(\pm 4)$ km/s per MW rf power. V_{pol} is calculated from the measured Doppler shift of Ar^{16+} forbidden z (3994.4 mÅ) and w (3949.4 mÅ) lines by a high resolution x-ray spectrometer (HIREX)[46] (Fig. 13). Because of the high collisional frequency in typical Alcator C-Mod plasmas, the impurity ion velocity is close to the bulk plasma ion velocity. Unfortunately, in these experiments, only one of the three

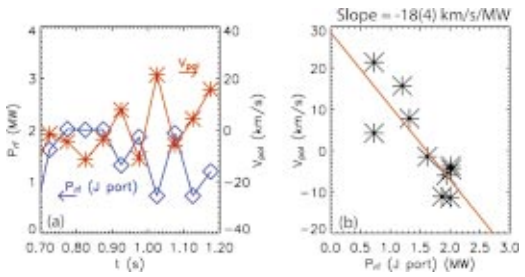

FIG. 12. (Color) V_{pol} vs rf power. $B_t=7.8$ T, $n_{e0}\simeq 1.7\times 10^{20}$ m^{-3}, $I_p=800$ kA, $T_{e0}\simeq 3.5$ keV. Estimated species concentrations: $n_H/n_e\simeq 0.06$, $n_D/n_e\simeq 0.78$ and $n_{^3\mathrm{He}}/n_e\simeq 0.08$.

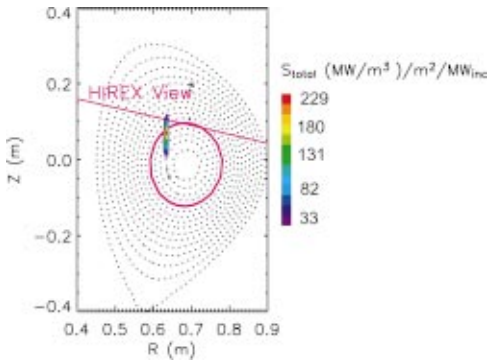

FIG. 13. (Color) HIREX viewing chord and the 2D S_{eld} from TORIC ($n_\phi = 7$). A strong MC power deposition region near the HIREX viewing flux surface.

chords of this HIREX array was available. This chord views a magnetic surface that intersects the midplane at $R \simeq 0.57$ m on the HFS as shown in Fig. 13. V_{pol} has an unknown offset due to the lack of absolute calibration. The rf effect is inferred from the correlation between the velocity and the modulated rf power. We estimate the MC layer from the break in slope in ECE signals from a nine-channel grating polychromator with a radial resolution of about 3 cm. The MC layer is found to be on the HFS at $R \simeq 0.62$ m, and the MC power is about 300 kW for 2 MW total rf power. The species mix is $n_{\mathrm{H}}/n_e \simeq 0.06, n_D/n_e \simeq 0.78$ and $n_{^3\mathrm{He}}/n_e \simeq 0.08$, calculated using the MC layer location and the measured H/D ratio. In Fig. 13, we also plot the 2D power deposition contours from TORIC simulation using the experimental plasma parameters ($n_\phi = +7$), which shows a small region with strong MC power deposition near the magnetic flux where the HIREX chord views. Therefore, the correlation shown in Fig. 12(b) might result from the MC flow drive. The negative slope indicates the rf effect is in the electron diamagnetic drift direction on this flux surface for this plasma. In two adjacent discharges with nearly identical plasma parameters but different antenna phasing, the correlation between the poloidal velocity and the rf power also exists. In discharge 10 307 160 19 with $[0,\pi,\pi,0]$ phasing, $v_{\mathrm{pol}} \simeq -22(\pm 5)$ km/s per MW rf power, while in discharge 10 307 160 21 at co-current drive phasing, $v_{\mathrm{pol}} \simeq 11$ (± 4) km/s per MW rf power. Some experiments in H(^{3}He,D) plasmas have also been performed, but the result is inconclusive due to the operational difficulty in obtaining a desirable species mix. The preliminary result reported here with velocity measurement at a single spatial location is inadequate to benchmark with theoretical or numerical models, such as Ref. 14, but rather a preliminary experimental evidence of rf correlated, possibly rf driven, flow near the MC layer. More experiments in plasmas with stronger MC and with better diagnostics, including an upgraded PCI system for wave measurement, are planned in Alcator C-Mod in the near future.

V. SUMMARY

The MC ICW was observed for the first time in tokamak plasmas in Alcator C-Mod using a PCI system. The wave is on the LFS of the ion–ion hybrid layer, and it has wavelength generally between the MC IBW and fast wave. Detailed measurement of the MCEH in D(H) plasmas with moderate H concentration and comparison with TORIC modeling shows that the MC ICW can have comparable contribution to that of MC IBW in electron heating when the mode conversion is off axis. Preliminary experimental evidence of rf correlated poloidal flow near the MC location is also reported.

ACKNOWLEDGMENTS

The authors thank the Alcator C-Mod operations for running the tokamak.

This work is supported at MIT by U.S. DOE Cooperative Agreement No. DE-FC02-99ER54512.

[1] R. Majeski, C. K. Phillips, and J. R. Wilson, Phys. Rev. Lett. **73**, 2204 (1994).
[2] R. Majeski, J. H. Rogers, S. H. Batha *et al.*, Phys. Rev. Lett. **76**, 764 (1996).
[3] Y. Takase, R. L. Boivin, F. Bombarda *et al.*, Plasma Phys. Controlled Fusion **38**, 2215 (1996).
[4] P. T. Bonoli, M. Brambilla, E. Nelson-Melby *et al.*, Phys. Plasmas **7**, 1886 (2000).
[5] P. T. Bonoli, P. O'Shea, M. Brambilla *et al.*, Phys. Plasmas **4**, 1774 (1997).
[6] J.-M. Noterdaeme, S. Wukitch, D. A. Hartmann *et al.*, in *Proceedings of the 16th IAEA Fusion Energy Conference* (IAEA, Vienna, 1996), pp. IAEA-CN-64/E1-EP-4.
[7] B. Saoutic, A. Bécoulet, T. Hutter, A. K. Ram, and A. Bers, Phys. Rev. Lett. **76**, 1647 (1996).
[8] M. J. Mantsinen, M.-L. Mayoral, E. Righi *et al.*, in *14th Topical Conference on Radio Frequency Power in Plasmas* (American Institute of Physics, New York, 2001), Vol. 595 of AIP Conference Proceedings, p. 59.
[9] C. K. Phillips, M. G. Bell, R. E. Bell *et al.*, Nucl. Fusion **40**, 461 (2000).
[10] T. H. Stix, *Waves in Plasmas* (American Institute of Physics, New York, 1992).
[11] F. W. Perkins, Nucl. Fusion **17**, 1197 (1977).
[12] E. Nelson-Melby, M. Porkolab, P. T. Bonoli, Y. Lin, A. Mazurenko, and S. J. Wukitch, Phys. Rev. Lett. **90**, 155004 (2003).
[13] D. W. Faulconer, D. V. Eester, and R. R. Weynants, in *Proceedings of the 14th EPS Conference on Controlled Fusion and Plasma Physics* (European Physical Society, Petit-Lancy, 1987), Vol. 11D, p. 932.
[14] E. F. Jaeger, L. A. Berry, J. R. Myra *et al.*, Phys. Rev. Lett. **90**, 195001 (2003).
[15] Y. Lin, S. J. Wukitch, P. T. Bonoli *et al.*, Plasma Phys. Controlled Fusion **45**, 1013 (2003).
[16] J. R. Myra and D. A. D'lppolito, Phys. Plasmas **9**, 3867 (2002).
[17] A. G. Elfimov, G. A. Segundo, R. M. O. Galvao, and I. C. Nascimento, Phys. Rev. Lett. **84**, 1200 (2000).
[18] E. F. Jaeger, L. A. Berry, and D. B. Batchelor, Phys. Plasmas **7**, 641 (2000).
[19] J. R. Myra and D. A. D'lppolito, Phys. Plasmas **7**, 3600 (2000).
[20] L. A. Berry, E. F. Jaeger, and D. B. Batchelor, Phys. Rev. Lett. **82**, 1871 (1999).
[21] B. P. LeBlanc, R. E. Bell, S. Bernabei *et al.*, Phys. Rev. Lett. **82**, 331 (1999).
[22] R. Cesario, A. Cardinali, C. Castaldo *et al.*, Phys. Plasmas **8**, 4721 (2001).
[23] B. LeBlanc, S. Batha, R. Bell *et al.*, Phys. Plasmas **2**, 741 (1995).
[24] P. Terry, Rev. Mod. Phys. **72**, 109 (2000).
[25] J. D. Moody, M. Porkolab, C. L. Fiore *et al.*, Phys. Rev. Lett. **60**, 298 (1988).
[26] I. H. Hutchinson, R. Boivin, F. Bombarda *et al.*, Phys. Plasmas **1**, 1511 (1994).
[27] Y. Takase, S. N. Golovato, M. Porkolab, K. Bajwa, H. Becker, and D. Caldwell, in *Proceedings of the 14th IEEE/NPSS Symposium on Fusion Engineering* (IEEE, Piscataway, NJ, 1992), p. 118.
[28] S. J. Wukitch, R. L. Boivin, P. T. Bonoli *et al.*, in *Proceedings of the 19th IAEA Fusion Energy Conference* (IAEA, Vienna, 2002), pp. FT/P1–14.

[29]A. Mazurenko, M. Porkolab, D. Mossessian, J. A. Snipes, X. Xu, and W. Nevins, Phys. Rev. Lett. **89**, 225004 (2002).
[30]H. Weisen, Rev. Sci. Instrum. **59**, 1544 (1988).
[31]F. F. Chen, *Introduction to Plasma Physics and Controlled Fusion* (Plenum, New York, 1984).
[32]A. K. Ram and A. Bers, Phys. Fluids B **3**, 1059 (1991).
[33]M. Brambilla, *Kinetic Theory of Plasma Waves, Homogeneous Plasmas* (Clarendon, Oxford, 1998).
[34]M. Brambilla, Nucl. Fusion **38**, 1805 (1998).
[35]M. Brambilla, Plasma Phys. Controlled Fusion **41**, 1 (1999).
[36]T. H. Stix, Nucl. Fusion **15**, 737 (1975).
[37]E. Nelson-Melby, Ph.D. thesis, Massachusetts Institute of Technology, 2001.
[38]P. O'Shea, Ph.D. thesis, Massachusetts Institute of Technology, 1997.
[39]G. Taylor, B. LeBlanc, C. K. Phillips *et al.*, in *13th Topical Conference on Radio Frequency Power in Plasmas* (American Institute of Physics, New York, 1999), Vol. 485 of AIP Conference Proceedings, p. 490.
[40]I. Manakhov, Y. Petrov, V. Basiuk, A. Bécoulet, and F. Nguyen, in Ref. 39, p. 136.
[41]C. K. Phillips, P. T. Bonoli, J. C. Hosea *et al.*, in *12th Topical Conference on Radio Frequency Power in Plasmas* (American Institute of Physics, New York, 1997), Vol. 403 of AIP Conference Proceedings, p. 265.
[42]T. E. Tutt, Master's thesis, Massachusetts Institute of Technology, 1999.
[43]D. J. Gambier, M. P. Evrarda, J. Adam *et al.*, Nucl. Fusion **30**, 23 (1990).
[44]L. Lao, H. S. John, R. Stambaugh *et al.*, Nucl. Fusion **25**, 1611 (1985).
[45]J. W. Heard, C. Watts, R. F. Gandy, and P. E. Phillips, Rev. Sci. Instrum. **70**, 1011 (1999).
[46]J. E. Rice and E. S. Marmar, Rev. Sci. Instrum. **61**, 2753 (1990).